CHARGED PARTICLE PRODUCTION AT THE CERN-ISR

G. GIACOMELLI

INTRODUCTION

The CERN Intersecting Storage Rings (ISR) give us a unique opportunity to investigate proton-proton collisions up to 52 GeV in the centre-of-mass system, corresponding to 1500 GeV = 1.5 TeV for a proton beam colliding with a stationary proton. One can thus study phenomena in a completely new energy region, which could only be glimpsed until now in cosmic rays. In about one year of operation the ISR has yielded significant results in elastic scattering and in the simplest particle production reactions.

In this lecture I shall first give a brief review of the characteristics of the CERN-ISR and of the experiments being performed there at present. Then I shall give the experimental results on the production of charged particles at the ISR and compare them with lower energy data and with the predictions of some theoretical models. The production of neutral particles at the ISR and a review of the cosmic-ray data are discussed in these Proceedings by Schubert and Levecque respectively[1,2].

THE ISR

Figure 1 shows the general layout of the ISR. The protons accelerated by the CERN Proton Synchrotron (PS) are stored first in one

ring and then in the other. The two rings intersect eight times; the experiments may be performed around these eight intersecting regions. Table 1 gives some of the main parameters of the ISR, in particular those quantities which are important for experimentalists.

Table 1

Some parameters of the CERN-ISR

Maximum energy of each beam	28 GeV
Average radius of each ring	150 m
Number of intersections	8
Intersection angle at crossing regions	14.79°
Lengths of long straight sections	16.8 m
Design value of beam current in each ring	20 A
Present value of beam current in each ring	3-7 A
Design luminosity	4×10^{30} cm^{-2} sec^{-1}
Maximum luminosity achieved so far	$\simeq 5 \times 10^{29}$ cm^{-2} sec^{-1}
Present collision rate in each region	$\simeq 2 \times 10^{4}$ interactions/sec
Average pressure in ISR	$\leq 10^{-9}$ Torr
Pressure in intersections	10^{-11}-10^{-12} Torr
Transverse beam dimensions horizontal	$\sim$ 7 cm
Transverse beam dimensions vertical	$\sim$ 1 cm
Beam lifetime at 2 A	$\sim$ 1 month
Beam lifetime at 6 A	$\sim$ 1 day
Max. magnetic field at equilibrium orbit	12 kG
Radio frequency	9.53 MHz
Harmonic number	30

The two beams have a ribbon shape, 7 cm horizontal and 0.5-1 cm vertical; therefore the interaction region is "diamond shaped" (in practice, considering the non-uniform population of the ribbon, "potato shaped"), with a total length of almost 60 cm and a height of 0.5-1 cm. At present four energies are operational:

2×11.5 GeV/c corresponding to 250 GeV/c in the lab.
2×15.3 GeV/c corresponding to 500 GeV/c in the lab.
2×22.5 GeV/c corresponding to 1000 GeV/c in the lab.
2×26.5 GeV/c corresponding to 1500 GeV/c in the lab.

The ISR started operating one year ago. The machine is being improved continuously; therefore some of the values quoted in Table 1 may rapidly become obsolete. In particular the machine people are systematically removing the pressure pockets, which seem to be responsible for the increase in loss rates with respect to stored beam intensities. It may also be possible to reach 2×31 GeV/c corresponding to about 2 TeV.

The main advantage of the ISR is connected with the large energies one may obtain, because the c.m. system is essentially coincident with the lab. system. The drawbacks of the ISR are the relatively low collision rates and the experimental limitations connected with being able to study only proton-proton collisions.

The total collision rate N in one intersection is given by

$$N = L\sigma_{tot} , \qquad (1)$$

where σ_{tot} is the total cross-section and L is the luminosity (the luminosity is that number which multiplied by the cross-section gives the number of events per unit time). Since $\sigma_{tot}(pp) \simeq 40$ mb and $L \simeq 5 \times 10^{29}$ cm^{-2} sec^{-1} (at present), the total collision rate is $N \simeq 2 \times 10^{4}$ particles per second. This value is about 10^5 times smaller than for a conventional accelerator. At 26×26 GeV/c the average multiplicity is larger than ten; therefore one has more than 2×10^{5} particles produced per second in each region.

The measurement of the luminosity is one of the most crucial measurements at the ISR, since on it depends the knowledge of the absolute value. The luminosity is given explicitly as

$$L = \frac{I_1 I_2}{e^2 c h_{eff} \operatorname{tg} \alpha/2} , \qquad (2)$$

where I_1 and I_2 are the beam currents in rings 1 and 2; $\alpha = 14.79^{\circ}$ and the effective overlap height h_{eff} of the beams is

$$\frac{1}{h_{eff}} = \frac{\int S_1(z)S_2(z)\,dz}{\int S_1(z)\,dz \cdot \int S_2(z)\,dz} , \tag{3a}$$

where $S_1(z)$ and $S_2(z)$ are the normalized vertical distributions of each beam.

In practice h_{eff} is measured by the Van Der Meer method[3] of displacing the two beams vertically with respect to one another and registering the number of beam-beam coincidences with a monitor (Fig. 2). One has

$$h_{eff} = \frac{\Sigma(MM)}{(MM)_{max}} . \tag{3b}$$

The monitor is then calibrated and used to determine the absolute value of the cross-sections. The monitor constant K is defined as

$$K = \frac{I_1 I_2 t}{h_{eff} MM_{max}} = \frac{I_1 I_2 t}{\Sigma(MM)} , \tag{4}$$

where t is the length of time for taking one point in the curve of Fig. 2.

The cross-section σ for the production of ΔN particles into the solid angle $\Delta\Omega$ and with the momentum band Δp is given by

$$\frac{d^2\sigma}{d\Omega dp} = \frac{\Delta N}{\Delta t \cdot L \cdot \Delta\Omega\Delta p} . \tag{5a}$$

In terms of the monitor constant K and with practical units one has

$$\frac{d^2\sigma}{d\Omega dp}\left[\text{mb/sr (GeV/c)}\right] \simeq \frac{\Delta N}{100 \cdot \Delta\Omega\Delta p \cdot K \cdot MM} , \tag{5b}$$

where Δt is the duration of the run and MM is the number of monitor events recorded during the time Δt.

3. THE PRESENT EXPERIMENTAL PROGRAM AT THE ISR

The experiments at present in progress at the ISR are given in Table 2. It may be interesting to remark that about a dozen experiments are going on at the same time in five intersections. These experiments may be classified as first generation experiments even

Table 2

Experiments in progress at the CERN-ISR

Intersection	Code	Collaboration	Experiment	Method	Angular region
1	R101	Bombay-Bucharest-CERN-Cracow	Production of charged particles	Emulsion	Around 90°
	R102	Saclay-Strasbourg	Production of $\pi^{\pm}$, $K^{\pm}$, $p^{\pm}$, γ, $e^{\pm}$, quarks	Magnetic spectrometer	Around 90°
	R103	CERN-Columbia-Rockefeller	Search for massive di-leptons ($e^{+}e^{-}$, γ)	Pb glass Čerenkovs	Around 90°
	Test	Brookhaven-Grumman-Rome	Search for magnetic monopoles	Pb glass Čerenkovs	Around 90°
2	R201	CERN-Lancaster-Manchester	Production of $\pi^{\pm}$, $K^{\pm}$, $p^{\pm}$	Magnetic spectrometer	20-150 mrad
	R202	ANL-Bologna-Michigan-Saclay	Production of $\pi^{\pm}$, $K^{\pm}$, $p^{\pm}$	Magnetic spectrometer	80-350 mrad
	R203	British-Scandinavian	Production of $\pi^{\pm}$, $K^{\pm}$, $p^{\pm}$	Magnetic spectrometer	30°-90°
	R204	British	$W^{\pm}$ search (wide angle $\mu^{\pm}$)	Iron plates	Around 90°
4	R402	CERN-Munich	Search for quarks	Counters, dE/dx	10°-30°
	Test	CERN-Hamburg-Vienna	Production of γ	Pb glass Čerenkovs	10°-90°
	Test	CERN-Hamburg-Vienna	Production of charged particles	Spark chambers	30°-90°
	R401	CERN-Hamburg	Isobar production ($pp \rightarrow p + N^{*}$)	Pb glass Čerenkovs	10°-90°
	Test	CERN-Karlsruhe	Production of neutrons	n-calorimeter	10°-30°
	Test	Aachen-CERN-Munich	Production of multiparticles	Projection chambers	Around 90°
6	R601	CERN-Rome	$pp \rightarrow pp$, CN-C interference	Counters	2-20 mrad
	R602	Aachen-CERN-Genoa-Turin	$pp \rightarrow pp$, diffraction	Magnetic spectrometer	$0.04 < \lvert t \rvert < 0.50$
	Test	Aachen-CERN-Genoa-Turin	Production of charged particles	Counters	50°-90°
8	R801	Pisa-Stony Brook	$\sigma_{tot}(pp)$, correlations	Counters	2°-90°

if most of them are rather complex. The second generation experiments should start in 1973, when a large magnet (the split field magnet) will be placed around the intersection region number 4.

Table 2 indicates that the experimental program includes measurements of the total cross-section, of elastic scattering and of particle production (including the production of as yet unobserved objects). Essentially all the particle production experiments are still studying the simplest inclusive reactions of the type

$$p + p \rightarrow c + X \ , \qquad (6)$$

where only the particle c is observed and X denotes all the non-detected reaction products. c may be a pion or kaon or γ, n, $\mu^{\pm}$, $p^{\pm}$, $e^{\pm}$, etc. A first look at correlations in inclusive reactions will be made in the near future and it is expected that the split-field magnet facility will bring into full swing this type of measurement.

From an experimenter's point of view the ISR presents problems of utilization which are different from those of a normal accelerator. In fact the experiments and the machine are intimately intermingled so that beam intensity, beam positioning, beam stability, lifetime and background may be affected by the experimenter's equipment. Also the presence of so many experimenters, with conflicting requirements, makes the operation of the machine a complex one, which probably would have been impossible without the help of computers and advanced equipment.

4. CHARGED PARTICLE PRODUCTION AT THE ISR

The present interest in the study of inclusive processes of type (6) has been stirred up by many theoretical suggestions or models like the scaling hypothesis of Feynman[4], the limiting distribution hypothesis of Benecke et al.[5] and many specific particle production models. I refer to the other talks of these "Rencontres" and to the Proceedings of recent conferences for further theoretical and experimental discussions[6].

4.1 Experiments

The three main experiments on charged particle production at the ISR are performed in the intersection region number 2. The other experiments in regions 1, 4, and 6 obtain data as by-products of other measurements.

Figure 3 shows the general layout of the intersection region number 2. Figure 4 shows in more detail the layout of the medium angle spectrometer and the location of the small angle monitors. The intersection region 2 is completely crowded with experimental equipment for four experiments and for the common monitoring facilities. The layout and the equipment of the medium angle spectrometer are simple; the form of the spectrometer is nevertheless typical of that for any single-arm spectrometer experiment at the ISR. Particles produced at the interaction "diamond" with a particular angle and momentum are steered by the first two magnets B_1 and B_2 onto the axis of the first counter telescope $S_1C_1C_2C_3S_2S_3$. The momentum analysis is performed by the magnet B_3, which bends the particles vertically into the second counter telescope S_4S_5H. (In practice H is now made of a three-counter hodoscope.) A pion is identified by the coincidence $\pi = AC_1C_2$, where A is the sixfold coincidence $A = (S_1S_2S_3)(S_4S_5H)$ and C_1, C_2 are the outputs of gas threshold Čerenkov counters set at a pressure slightly above the pion knee. Similarly kaons and protons are identified as $K = A\bar{C}_1\bar{C}_2C_3$ and $p = A\bar{C}_1\bar{C}_2\bar{C}_3$, where C_3 is set above the kaon knee. The time of flight between S_1 and H is recorded in order to have an extra check on the protons and to detect heavier mass particles. Because of the large decay rates, kaons are better detected with a shorter spectrometer (up to S_6). The raw data have to be corrected for absorption, decay, electron contamination, multiple scattering and beam-gas interactions. The background coming from beam-gas and beam-walls interactions is small (2-20%), because the spectrometer is highly directional and because of the good vacuum in the intersection. The beam-gas background may be measured when only one beam is circulating in the ISR.

In other spectrometers it was found necessary to place their counters in coincidence with other large counters surrounding the beam

pipes (in the layout of Fig. 4 they would be placed at the position of the monitor counters, in particular as M_1). In this case beam-beam events are clearly selected and beam-gas events completely rejected. In order to really measure an inclusive process it is important that these coincidence counters detect the largest possible fraction of beam-beam events, since otherwise some correlation is introduced. In practice the coincidence counters collect between 50 and 90% of the interactions; checks on the distributions in different trigger conditions seem to indicate that no significant correlation is introduced. Nevertheless, we shall define these coincidence arrangements as measuring "almost inclusive" reactions.

4.2 Cross-sections and variables

As was discussed by many people at this meeting, many reference frames and many variables may be used to define inclusive reactions. We shall in general plot invariant cross-sections, that is

$$f = E\frac{d^3\sigma}{d^3\vec{p}} = \frac{E}{p^2}\frac{d^2\sigma}{d\Omega dp} = E\frac{d^2\sigma}{\pi dp_l dp_t^2} = \frac{1}{\pi}\frac{d^2\sigma}{dydp_t^2} \quad . \tag{7}$$

As independent variables we shall use (s,x,p_t) or (s,y,p_t); s is the square of the c.m. energy; p_l and p_t are the c.m. longitudinal and transverse momenta of the observed particle; x is the Feynman variable

$$x = \frac{p_l}{p_{l\,max}} = \frac{2p_l}{\sqrt{s}} \quad , \tag{8}$$

y is the rapidity variable :

$$y = \frac{1}{2}\ln\left(\frac{E + p_l}{E - p_l}\right) \xrightarrow[p_t^2 >> m^2]{} -\lg\ tg\ \frac{\theta}{2} \quad , \tag{9}$$

where m is the mass of the observed particles. For pions the measurement of the angle is sufficient to determine y, while this is not so for protons. We shall use $(y_{max} - y) = y_{lab}$ in our graphs.

The scaling hypothesis will be written as

$$f(s,x,p_t) \xrightarrow[s>>]{} f(x,p_t) \quad . \tag{10}$$

4.3 The results

Some of the most significant experimental results obtained so far at the ISR on charged particle production are shown in Figs. 5-10. Most of these results have still to be considered as preliminary, because they are based on first-order corrections only. A few words on experimental errors may be in order. The statistical errors are typically 4-10% for pions and protons and 10-25% for kaons and antiprotons. The corrections add point-to-point errors of about 5-10%. Therefore point-to-point errors are typically 7-15% for pions and protons, 10-20% for kaons and antiprotons. To these errors a systematic scale error, which may be estimated to be about 5-10%, has to be added. (This error arises mainly from the knowledge of the luminosity.) For comparison it is worth mentioning that the typical over-all errors of the lower energy data are about 10-15% [7].

Figure 5 shows the invariant cross-sections as a function of x, keeping p_t as a parameter[8-10]. The points indicate measurements at different ISR energies, while the shadowed bands and/or the solid lines represent interpolations at lower energies[11-14].

Figure 6 shows the negative pion data of Fig. 5 [9] plotted versus the difference in rapidity $(y_{p\,max} - y_c) = y_{lab}$. The rapidity variable expands and therefore allows a better study of the central region (or pionization region). It is apparent that the curves look rather regular in the y_{lab} variable. Moreover the data from different experiments superimpose correctly.

Figure 7 shows the cross-section $(d^2\sigma/d\Omega dp)$ around 90° plotted versus $(-\lg \operatorname{tg} \theta/2)$ [15]. In these experiments of the "almost inclusive" type, one detected charged particles, without knowing the sign and type. Therefore they can only be plotted versus an angular variable, which, as discussed before, is essentially the rapidity variable for pions. Both Figs. 6 and 7 indicate that the cross-sections seem to be flat as a function of y. Previous emulsion experiments[16] disagreed with these conclusions, while new results from the large angle spectrometers[17-19] seem to confirm them.

Figure 8 shows the pion, proton and antiproton production cross-sections at $\theta_{cm} = 90^\circ$ plotted as a function of p_t [18]. The distributions are well represented by exponential functions of the type

$$E \frac{d^3\sigma}{d^3\vec{p}} = Ae^{-bp_t} . \qquad (11)$$

The slopes are different for pions and nucleons (see Table 3). We shall define the average transverse momentum as

$$\langle p_t \rangle_{p_\ell} = \int_0^\infty p_t \left(E \frac{d^3\sigma}{d^3\vec{p}} \right) dp_t \Big/ \int_0^\infty \left(E \frac{d^3\sigma}{d^3\vec{p}} \right) dp_t , \qquad (12)$$

where $\langle p_t \rangle_{p_\ell}$ means that the cross-sections considered are for a fixed value of p_ℓ. One could also define $\langle p_t \rangle_\theta$ with cross-sections at a fixed production angle and $\langle p_t \rangle_x$ at fixed x. At 90° the three definitions coincide.

Table 3

The results of fitting the p_t-distributions for x = 0 at the total c.m. energy of 52 GeV to formula (11) [18]. The average value of the transverse momentum was computed using the definition (12). (The errors are purely statistical.) The British-Scandinavian group[17] finds b(π) = 6.4, b(p) = 5.3 and b($\bar{p}$) = 4.8

	π^+	π^-	p	$\bar{p}$
A	140 ± 4	141 ± 4	11.6 ± 1.2	5.6 ± 0.8
b	6.26 ± 0.07	6.24 ± 0.07	4.16 ± 0.13	4.0 ± 0.2
$\langle p_t \rangle$	359 ± 5	360 ± 5	670 ± 35	710 ± 45

Figures 9 and 10 show various particle ratios plotted versus x for p_t = 0.4 GeV/c [10,20]. The ratios involve particles of the same sign (K^-/π^-, $\bar{p}/\pi^-$, K^+/π^+, p/π^+) as well as particles and antiparticles (π^+/π^-, K^+/K^-, $p/\bar{p}$). The solid lines in Figs. 9 and 10 represent interpolations through the 24 GeV/c data of Allaby et al.[11]. The average values of these ratios are tabulated in Table 4.

4.4 Discussion of the ISR results

On the basis of the experimental results shown in Figs. 5-10, one may make the following remarks:

Table 4

Average values of various particle ratios for p_t = 0.4 GeV/c and 0.1 < x < 0.4. (Errors include rough estimates of systematic uncertainties)

	ISR[10,20]	24 GeV [11]
$\bar{p}/\pi^-$	5.0 ± 1	0.7 ± 0.1
K^-/π^-	8.0 ± 1.5	4.2 ± 0.8
K^+/π^+	12.5 ± 1.8	9.5 ± 1.2

4.4.1 Pions

a) For 0.1 < x < 0.4 the x- and y-distributions for positive and negative pions at fixed values of p_t (at p_t = 0.2, 0.4, 0.8 GeV/c) are essentially independent of the primary proton energies, for laboratory energies larger than 19 GeV (see Figs. 4 and 5). This statement is valid within the experimental error of about ±15%.

b) For x < 0.1 and at the smallest values of p_t the situation seems to be more complex and probably there is some non-scaling between the bulk of the accelerator data at 12-28 GeV and the bulk of the ISR data. At 90°, that is at x = 0, there seems to be an increase of the differential cross-section versus energy (see Fig. 6 and the report of Schubert).

c) The angular distribution of all charged particles in the region around 90° may be fitted with a formula

$$\frac{1}{\sigma_{inel}} \left(\frac{d\sigma}{d\Omega}\right)_{cm} = A(E_{cm}) \sin^{-2} \theta_{cm} , \qquad (13)$$

where $A(E_{cm})$ = 0.21 sr^{-1} at E_{cm} = 30 GeV and 0.25 at E_{cm} = 52.7 GeV [15].

d) As regards the p_t-distributions at fixed values of x, the ISR distributions are similar to those measured at lower energies. One has some problems in comparing the average value of the transverse momentum with the values obtained at other energies, because of actual differences in definitions.

e) The π^+/π^- ratio decreases with decreasing x going from about two at x = 0.4 to one at x = 0.

4.4.2 Nucleons

a) The x-distributions of protons are different from the distibutions of any other particle. This is clearly due to the leading particle effects. Also protons seem to scale between PS and ISR energies. (See Fig. 5.)

b) The antiproton production cross-section has increased by about a factor of six between 24 GeV/c and ISR energies (see Figs. 9 and 10). The $\bar{p}/\pi^-$ ratio increased from about 0.7% at 24 GeV/c to 1-2% at 70 GeV/c and to 5% at the ISR.

c) Within the experimental errors there does not seem to be any increase in antiproton cross-section between the lowest and the largest ISR energies (see Figs. 9 and 10).

d) At x = 0 the p_t-distribution of protons and antiprotons have the same slopes, smaller than those for pions (see Fig. 8 and Table 3).

e) The $p/\bar{p}$ ratio shows a spectacular decrease with decreasing x.

4.4.3 Kaons

a) The K^- production cross-section has increased by about a factor of two between 24 GeV/c and ISR energies (see Fig. 9a and Table 3).

b) The K^+ production cross-section has probably had a slight increase compared with lower energy data.

c) Within large errors the K^+/K^- ratio is not too dissimilar to the π^+/π^- ratio.

4.4.4 General features

The general features of the particle production results may be summarized as follows:

a) Even at ISR energies pion production is the dominant process.

b) While, roughly speaking, scaling seems to hold for pions, protons and probably also for K^+ mesons for energies larger than 20-30 GeV/c, the antiproton and K^- production cross-sections at the ISR are larger

than at lower energies. On the other hand, there does not seem to be any real change between data at the lowest and the highest ISR energies. This may indicate that limiting distributions are reached at ISR energies. The limiting distributions (or the scaling regions) are reached at smaller energies for pions and protons than for kaons and antiprotons.

c) All the particle to antiparticle ratios of Fig. 8 decrease with x towards a value close to one at x = 0. This may indicate a kind of statistical production process in the region around x = 0.

COMPARISON WITH THEORETICAL MODELS

Over most of the measured range the hypotheses of scaling and of limiting distributions predict similar results. Both hypotheses agree with the bulk of the data at ISR energies. The agreement extends to lower energies for pions and protons.

Figure 11 shows the comparison of the negative pion data with the statistical model of Hagedorn et al.[21]: the agreement is quite good. The model predicts only approximate scaling, which cannot be tested with the present data. The agreement of the Hagedorn model with the ISR data is valid also for all the other particles including antiprotons and kaons. The comparison of experimental data with the Hagedorn model is particularly appealing to the experimentalists for the practical reason that this is the only model which has been carried out as far as to give complete numerical tables of predictions.

Most of the semi-empirical formulae found in the literature are ruled out by the present ISR results. These formulae fail to predict scaling and fail to predict kaons and/or antiproton production. As an example, Fig. 12 shows a comparison of the negative pion data with the model of Cocconi[22], which represents a modification of the original CPK formula. The absolute normalization of the Cocconi formula was achieved by arbitrarily using a value of σ_{inel} = 30 mb and assuming $\sigma(\pi^-\text{-production})$ = 10 mb. It is probably possible to rearrange this and the other formulae to incorporate the ISR results, but it is clear that the formulae may be useful only for interpolating data at various energies.

Acknowledgements

Most of the work reported here was done with the active collaboration of A. Bertin, A. Bussière, P. Capiluppi, A. Cristallini, M. D'Agostino-Bruno, R.J. Ellis, C. Maroni, F. Mercatali, R. Poe, L.G. Ratner, A.M. Rossi and G. Vannini.

I would also like to thank many colleagues at CERN for discussions and information.

REFERENCES

1) K. Schubert, Production of photons at the CERN-ISR, communication to these Rencontres.

2) A. Leveque, Experimental results on inclusive reactions at very high-energies, communication to these Rencontres.

3) S. Van der Meer, Calibration of the effective beam height in the ISR, Internal Report CERN-ISR-PO/68-31 (1968).

4) R.P. Feynman, Phys. Rev. Letters 23, 1415 (1969).

5) J. Benecke, T.T. Chou, C.N. Yang and E. Yen, Phys. Rev. 188, 2159 (1969).

6) See, for instance, the Rapporteurs' talks of M. Deutschmann, G. Giacomelli and H. Satz, at the 1971 Amsterdam International Conference on Elementary Particles.

7) A.N. Diddens and K. Schlüpmann, Particle production in proton-proton interactions, to be published in Landoldt-Börnstein (1972).

8) L.G. Ratner, R.J. Ellis, G. Vannini, B.A. Babcock, A.D. Krisch and J.B. Roberts, Phys. Rev. Letters 27, 68 (1971), and Proc. APS/DPF 1971 meeting at Rochester, N.Y.

9) A. Bertin, P. Capiluppi, A. Cristallini, M. D'Agostino-Bruno, R.J. Ellis, G. Giacomelli, C. Maroni, F. Mercatali, A.M. Rossi and G. Vannini, Phys. Letters 38 B, 260 (1972).

10) A. Bertin, A. Bussiere, P. Capiluppi, M. D'Agostino-Bruno, R.J. Ellis, G. Giacomelli, R. Poe, A.M. Rossi and G. Vannini, Particle production at the CERN-ISR, presented at the 1972 Oxford Conference on Strong Interactions at High Energy.

11) J.V. Allaby, F. Binon, A.N. Diddens, P. Duteil, A. Klovning, R. Meunier, J.P. Peigneux, E.J. Sacharidis, K. Schlüpmann, M. Spiegel, J.P. Stroot, A.M. Thorndike and A.M. Wetherell, CERN 70-12 (1970), and CERN-Rome Collaboration, private communication.

12) C.W. Akerlof, D.G. Crabb, J.L. Day, N.P. Johnsons, P. Kalbachi, A.D. Krisch, M.T. Lin, M.L. Marskak, J.K. Randolph, P. Schmueser, A.L. Read, K.W. Edwards, J.G. Asbury, G.J. Marmer and L.G. Ratner, Phys. Rev. D3, 645 (1971).

13) H. Boggild, K.H. Hansen and M. Suk, Nuclear Phys. B27, 1 (1971).

14) D.B. Smith, R.J. Sprafka and J.A. Anderson, Phys. Rev. Letters 23, 1064 (1969).
W.H. Sims, J. Hanlon, E.O. Salant, R.S. Panvini, R.R. Kinsly, T.W. Morris and L. Von Lindern, Pion spectra from the reaction $p + p \rightarrow \pi^{\pm} + X$ at 28.5 GeV, to be published in Nuclear Phys. B.

15) G. Barbiellini, M. Bozzo, P. Darriulat, G. Diambrini-Palazzi, G. De Zorri, M. Holder, A. McFarland, G. Maderni, P. Mery, S. Orito, J. Pilcher, C. Rubbia, G. Sette, A. Stande, P. Strolin and K. Tittel, Charged particle production at large angles, to be published.

16) Bombay-CERN-Cracow Collaboration, Phys. Letters 36 B, 611 (1971) and to be published.

17) British-Scandinavian collatoration, E. Lillethun et al., Invited paper at the 1972 Oxford Conference on Strong Interactions at High Energy.

18) A. Banner et al., Saclay-Strasbourg collaboration, private communication.

19) M. Braidenbach et al., Production of charged particles around 90°, private communication.

20) M.G. Albrow, D.P. Barber, A. Bogaerts, B. Bosnjakovic, J.R. Brooks, A.B. Clegg, F.C. Erné, C.N.P. Gee, A.D. Kanaris, A. Lacourt, D.H. Locke, P.G. Murphy, A. Rudge, J.C. Sens and F. Van der Veen, Particle production ratios at 21, 31, 45 and 53 GeV in the centre of mass, to be published.

21) R. Hagedorn and J. Ranft, Suppl. Nuovo Cimento 6, 169 (1968).
J. Ranft, Phys. Letters 31 B, 529 (1970).
S. Andersson and C. Daum, Program ISRPRO, CERN Computing Library (1969).

22) G. Cocconi, L.J. Koester and D.H. Perkins, Calculation of particle fluxes from proton synchrotrons of energy 10 to 1000 GeV, Univ. California preprint UCRL 10022, p. 167.
G. Cocconi, Nuclear Phys. B28, 341 (1971).

Figure captions

Fig. 1 : General layout of the CERN-ISR. The figure shows the Proton Synchrotron, the transfer lines, and the two storage rings with their eight intersection regions.

Fig. 2 : "Luminosity curve" obtained by recording the MM monitor rate (see Fig. 4) versus the relative displacement of the ISR beams.

Fig. 3 : Layout of the experiments in intersection region number 2. The figure indicates the location of the small angle spectrometer (where particles are bent vertically), of the medium and large angle spectrometers, and of the muon detector.

Fig. 4 : The layout of the medium angle particle production experiment in intersection region number 2 [10]. B_1-B_3 are bending magnets, S_1-S_6 and H are scintillation counters, C_1-C_3 are gas threshold Čerenkov counters. B_1 is a septum magnet designed so as to give a perturbation as small as possible to the circulating proton beams. The time of flight is measured between counters S_1 and H (ℓ = 33.8 m).

Fig. 5 : The invariant cross-section $E(d^3\sigma/d^3p)$ plotted versus x, keeping p_t as a parameter, for (a) negative particle[9,10] and (b) positive particle[8] production. The shadowed regions represent interpolations through data at 19-28 GeV/c [11-14], while the points are ISR measurements.

Fig. 6 : The invariant cross-section $E(d^3\sigma/d^3p)$ plotted versus the rapidity $y_{p\,max} - y_c = y_{lab}$ for π^- production[10].

Fig. 7 : Angular distributions in the c.m. system for all charged particles produced at large angles[15].

Fig. 8 : The invariant cross-section $E(d^3\sigma/d^3p)$ plotted versus p_t for $x = 0$ (90° data)[17,18].

Fig. 9 : Particle to antiparticle ratios[10,20]. The solid lines are interpolations of the data at 24 GeV/c [11].

Fig. 10 : Particle ratios: (a) K^-/π^- and $\bar{p}/\pi^-$; (b) K^+/π^+ and p/π^+ [10,20]. The solid lines are interpolations of the data at 24 GeV/c [11].

Fig. 11 : Comparison of the negative pion production data at the ISR with the predictions of a statistical model[21].

Fig. 12 : Comparison of the production of negative particles at the ISR with the predictions of the Cocconi semi-empirical formula[22].

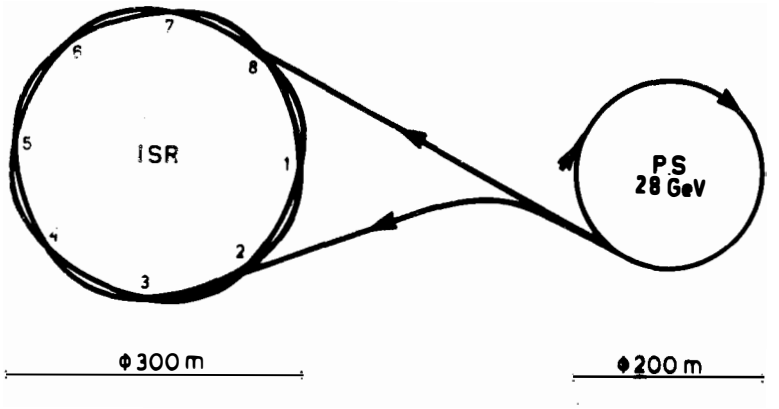
ISR
PS
28 GeV
Φ300 m
Φ200 m

Fig. 1

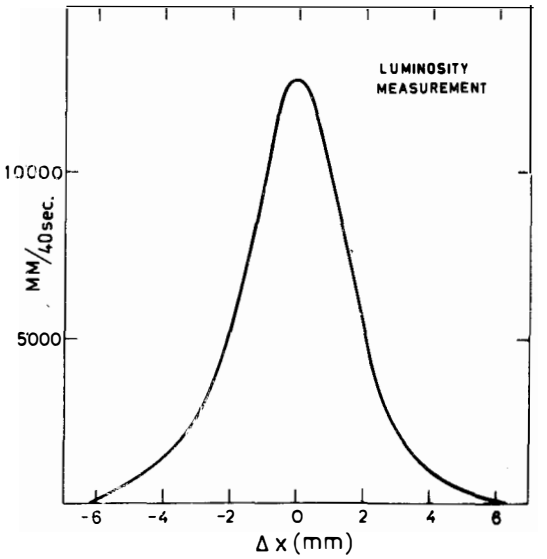
LUMINOSITY
MEASUREMENT
10000
5000
MM/40sec.
-6
-4
-2
0
2
4
6
Δ x (mm)

Fig. 2

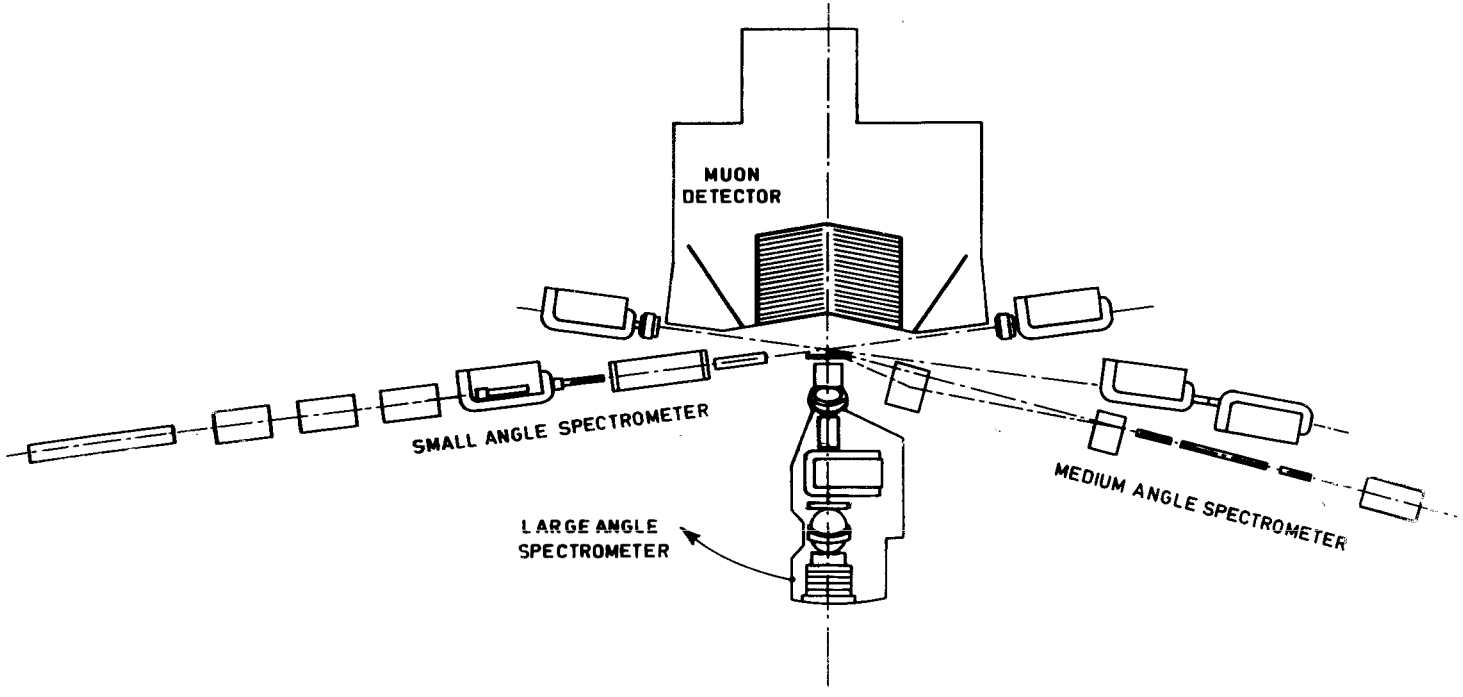
MUON
DETECTOR
SMALL ANGLE SPECTROMETER
MEDIUM ANGLE SPECTROMETER
LARGE ANGLE
SPECTROMETER

Fig. 3

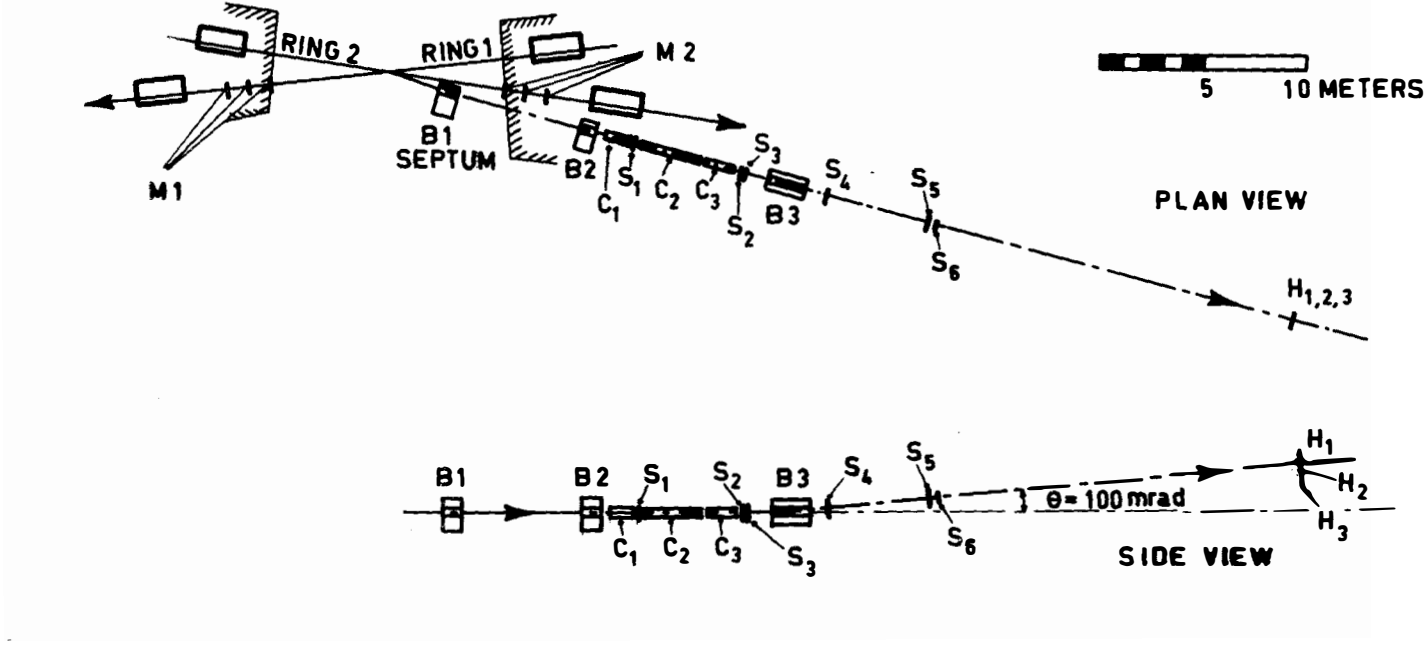
RING 2
RING 1
M 2
M 1
B1
SEPTUM
B2
B3
S_1
S_2
S_3
S_4
S_5
S_6
C_1
C_2
C_3
5
10 METERS
PLAN VIEW
$H_{1,2,3}$
B1
B2
B3
S_1
S_2
S_3
S_4
S_5
S_6
C_1
C_2
C_3
θ= 100 mrad
H_1
H_2
H_3
SIDE VIEW

Fig. 4

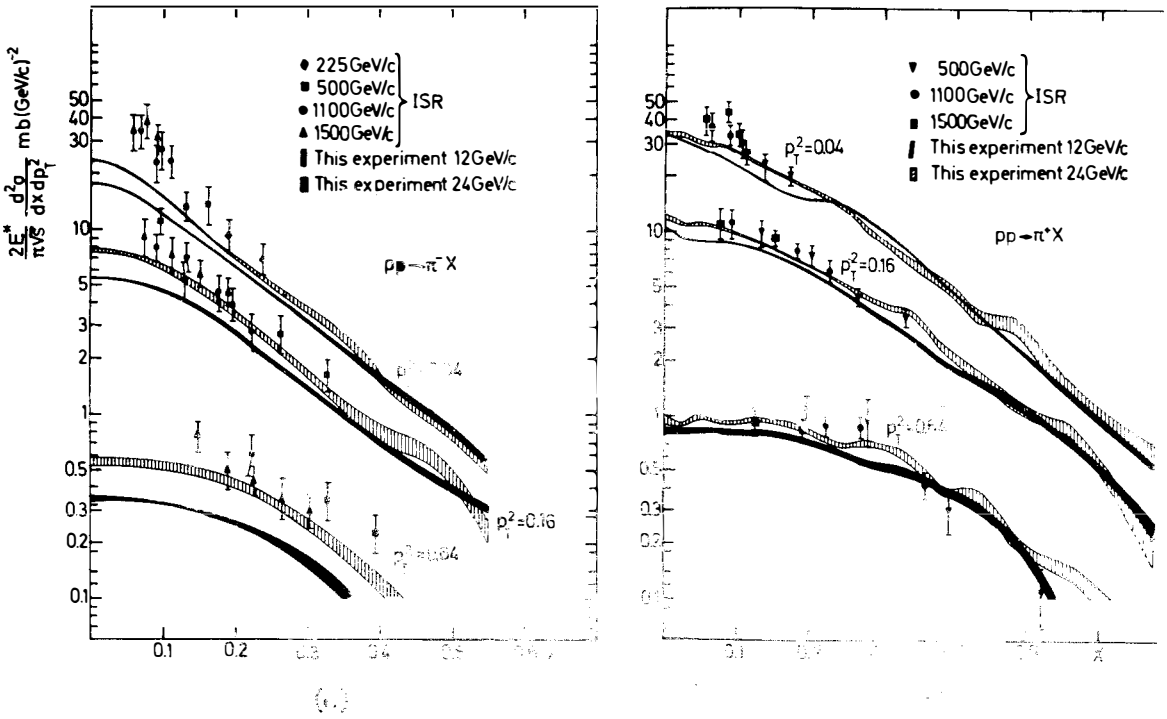
$\frac{2E^*}{\pi\sqrt{s}}\frac{d^2\sigma}{dx\,dp_T^2}$ mb(GeV/c)$^{-2}$
225GeV/c
500GeV/c
1100GeV/c
1500GeV/c
ISR
This experiment 12GeV/c
This experiment 24GeV/c
pp→π⁻X
p_T^2=0.16
pp→π⁺X
500GeV/c
1100GeV/c
1500GeV/c
ISR
This experiment 12GeV/c
This experiment 24GeV/c
p_T^2=0.04
p_T^2=0.16

Fig. 5

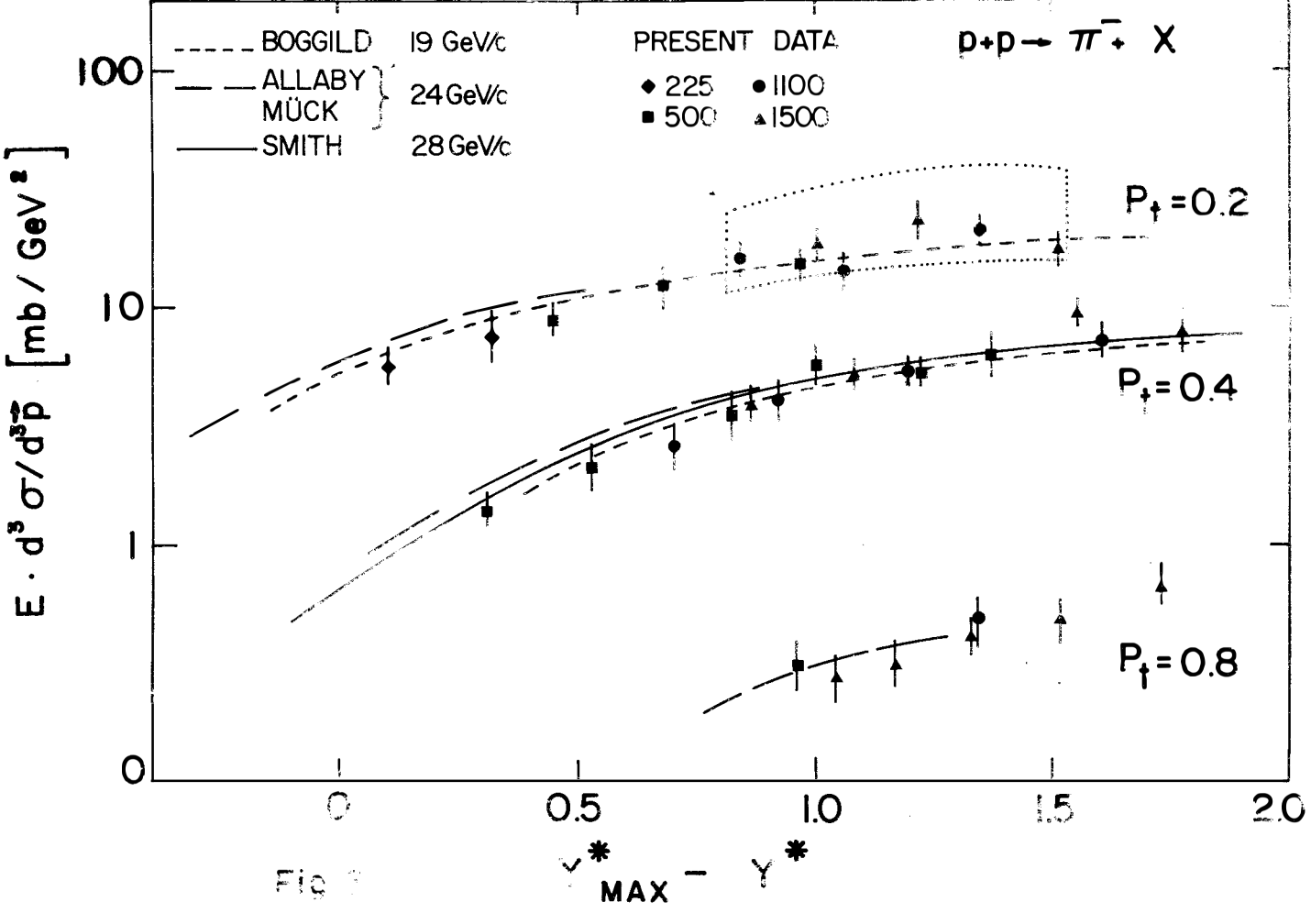
BOGGILD 19 GeV/c
ALLABY 24 GeV/c
MÜCK
SMITH 28 GeV/c
PRESENT DATA
225 1100
500 1500
p+p → π⁻ X
P_t = 0.2
P_t = 0.4
P_t = 0.8
E · d³σ/d³p̄ [mb / GeV²]
100
10
1
0
0
0.5
1.0
1.5
2.0
Y* MAX − Y*

Fig

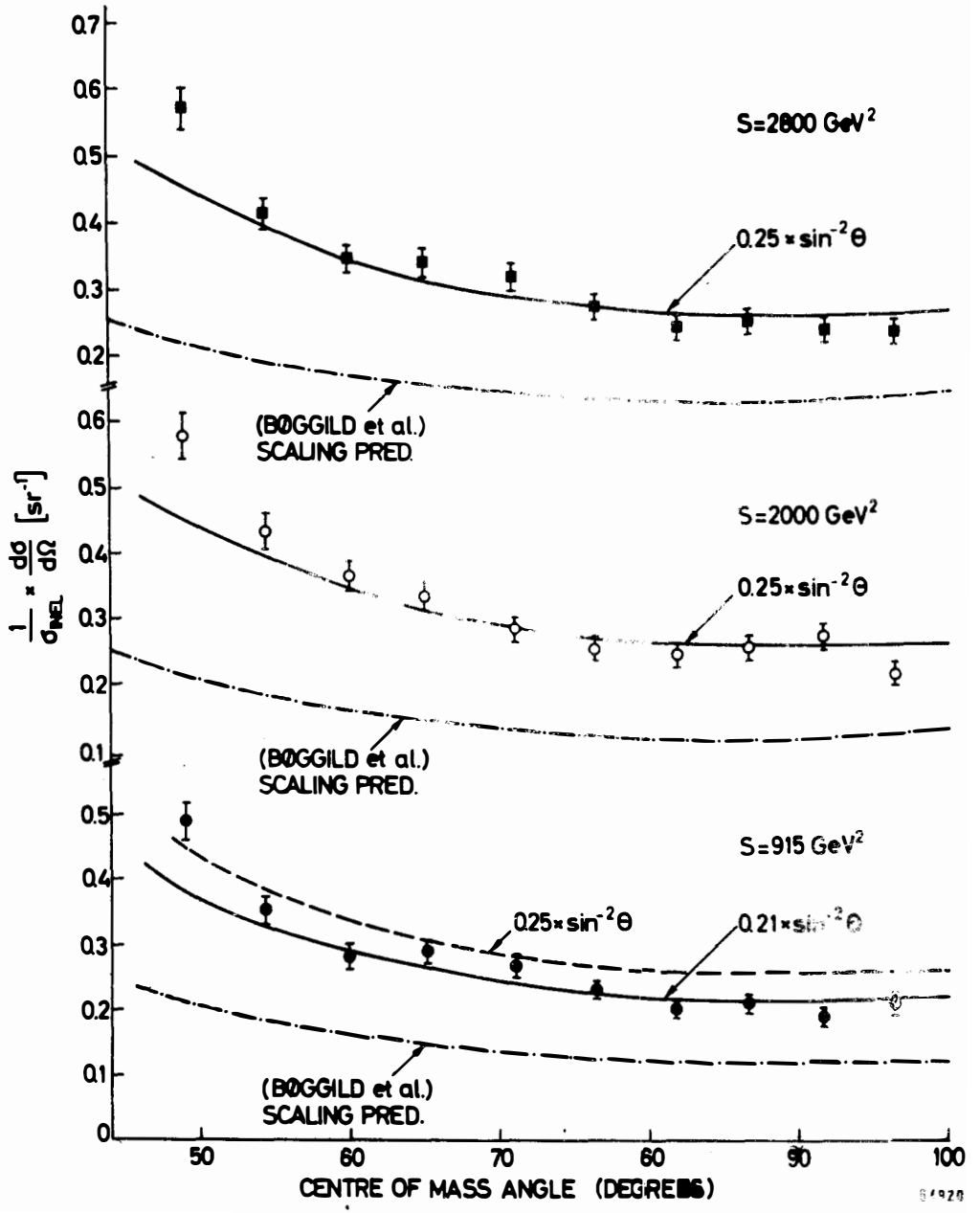
S=2800 GeV²
0.25×sin⁻²Θ
(BØGGILD et al.)
SCALING PRED.
S=2000 GeV²
0.25×sin⁻²Θ
(BØGGILD et al.)
SCALING PRED.
S=915 GeV²
0.25×sin⁻²Θ
0.21×sin⁻²Θ
(BØGGILD et al.)
SCALING PRED.
1/σ_NEL × dσ/dΩ [sr⁻¹]
CENTRE OF MASS ANGLE (DEGREES)

Fig. 7

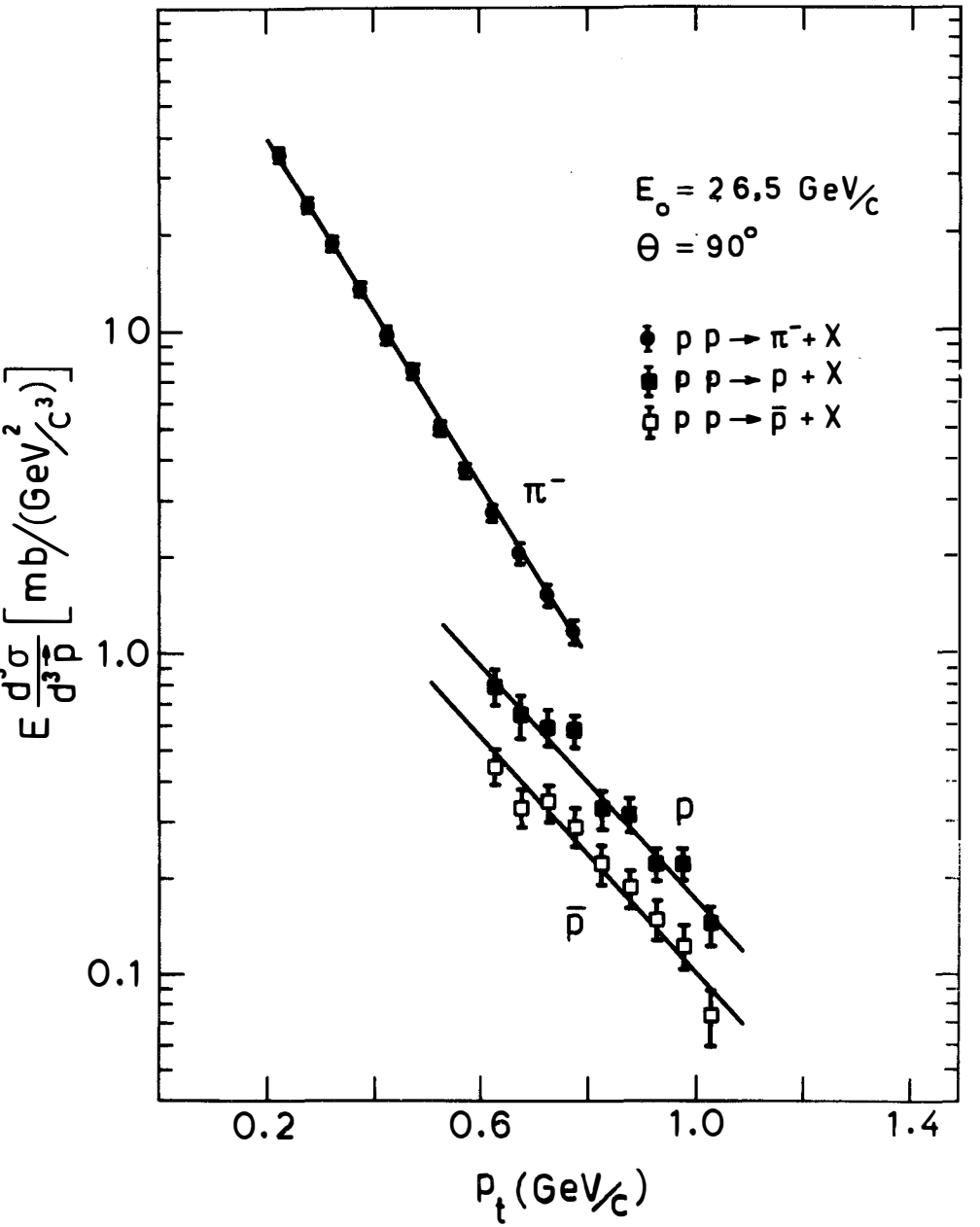
E_o = 26,5 GeV/c
Θ = 90°
p p → π⁻ + X
p p → p + X
p p → p̄ + X
π⁻
p
p̄
10
1.0
0.1
0.2
0.6
1.0
1.4
$E\frac{d^3\sigma}{d^3\vec{p}}\left[\frac{mb}{(GeV/c^3)^2}\right]$
p_t (GeV/c)

Fig. 8

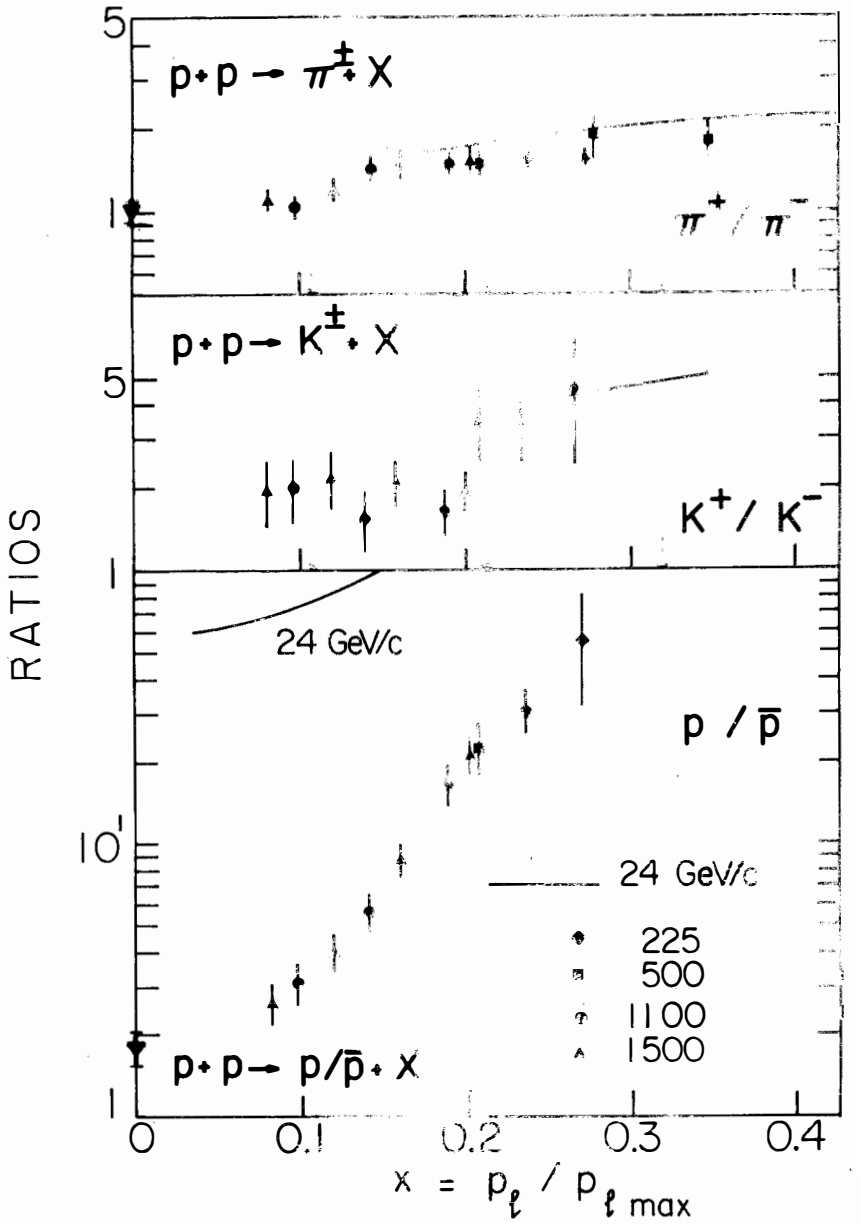
RATIOS
p + p → π± + X
π+ / π−
p + p → K± + X
K+ / K−
24 GeV/c
p / p̄
24 GeV/c
225
500
1100
1500
p + p → p/p̄ + X
5
1
5
1
10⁻¹
1
0
0.1
0.2
0.3
0.4
x = p_ℓ / p_ℓ max

Fig. 9

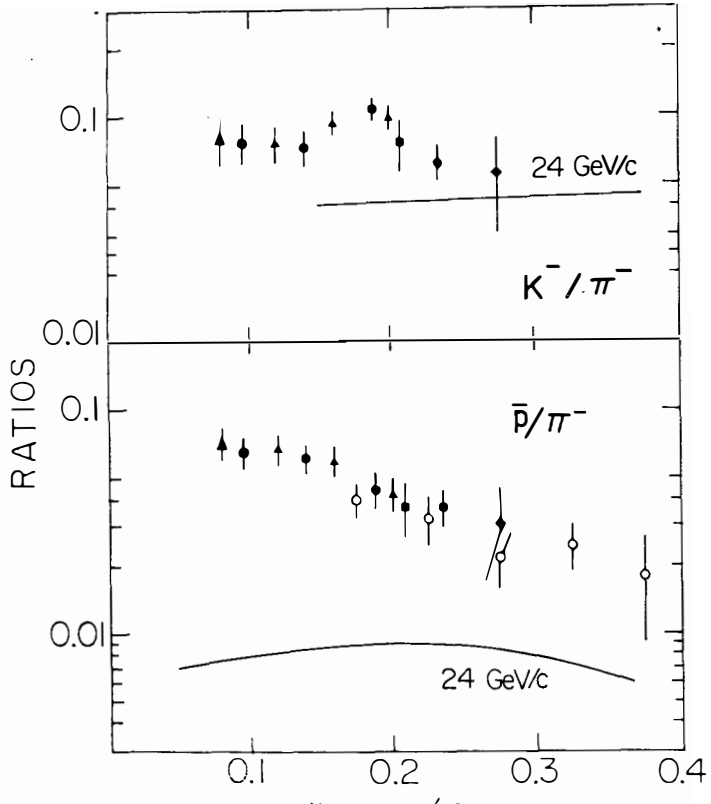

Fig. 10 a

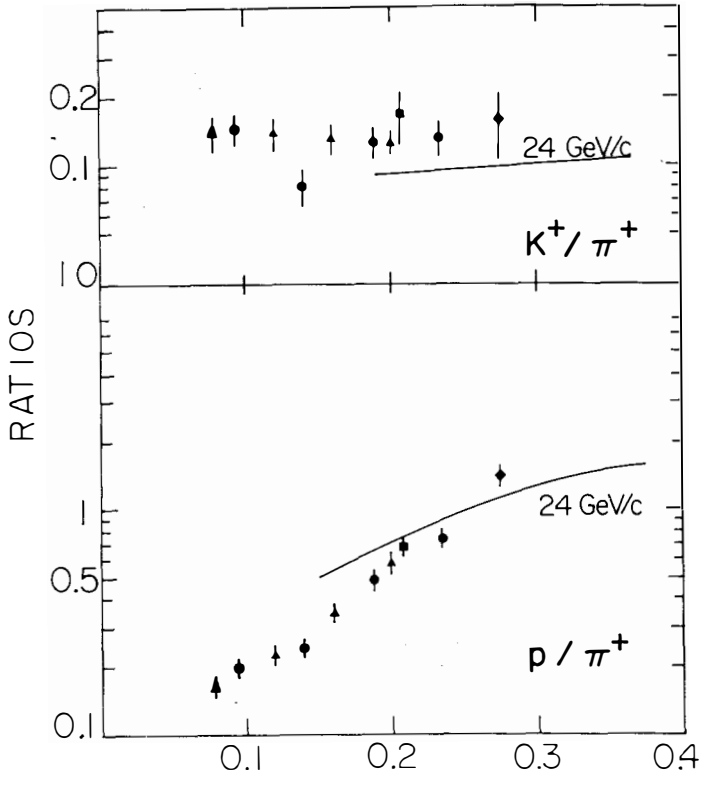

Fig. 10b

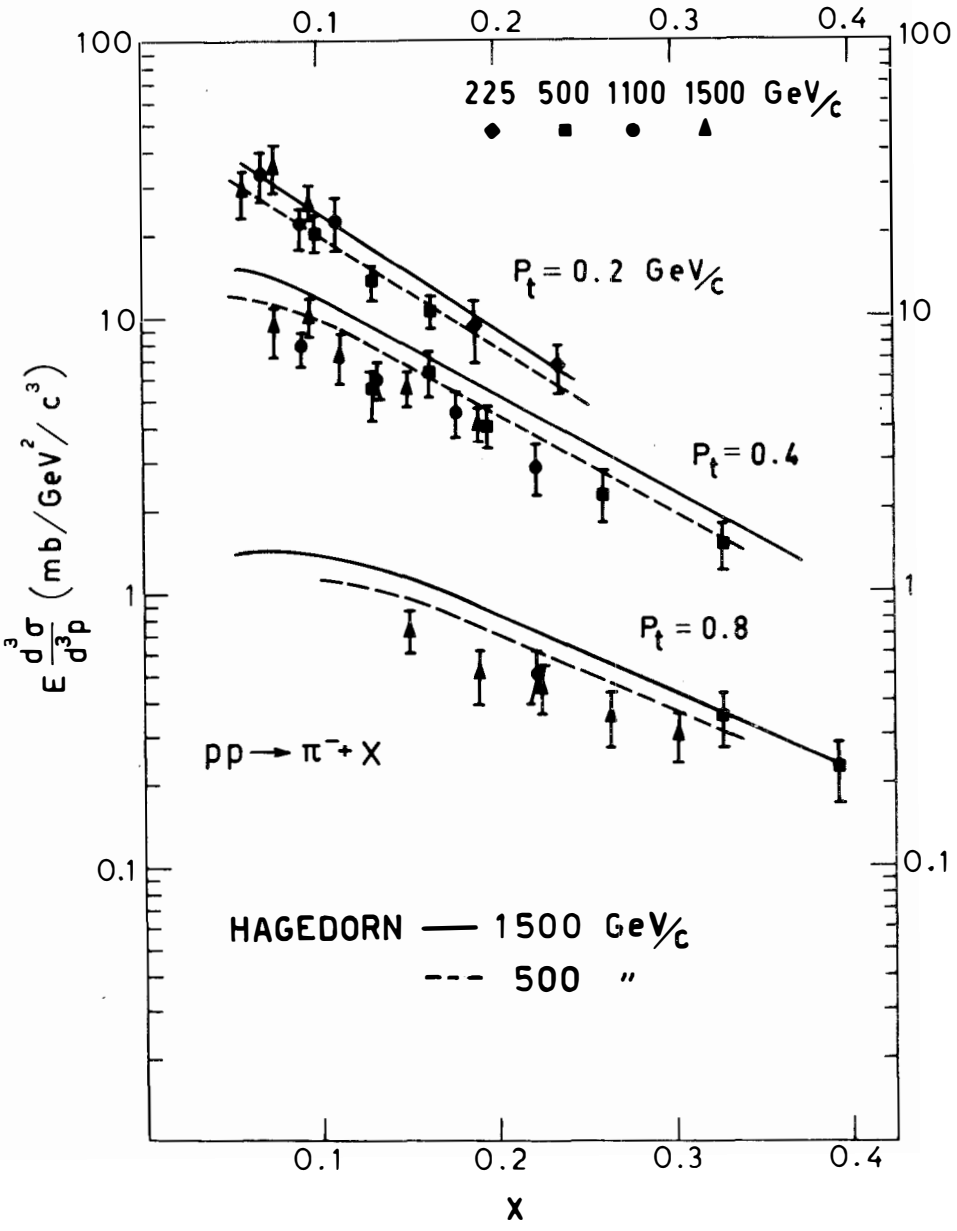
225 500 1100 1500 GeV/c
$P_t = 0.2$ GeV/c
$P_t = 0.4$
$P_t = 0.8$
$pp \rightarrow \pi^- + X$
HAGEDORN —— 1500 GeV/c
--- 500 "
$E\frac{d^3\sigma}{d^3p}$ (mb/GeV^2/c^3)
X
100
10
1
0.1
0.1
0.2
0.3
0.4

Fig. 11

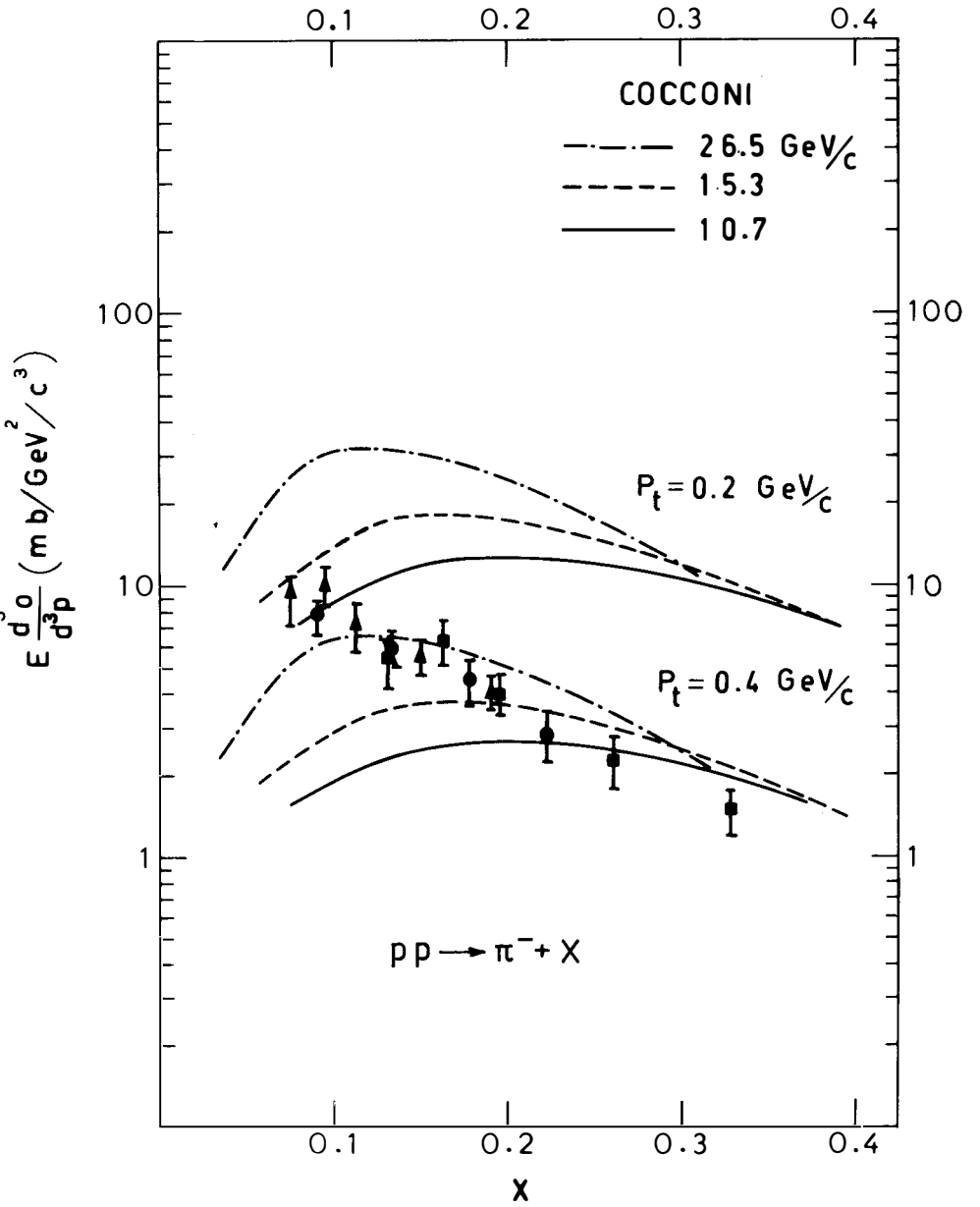
COCCONI
26.5 GeV/c
15.3
10.7
$P_t = 0.2$ GeV/c
$P_t = 0.4$ GeV/c
$pp \rightarrow \pi^- + X$
$E\frac{d^3\sigma}{d^3p}\left(mb/GeV^2/c^3\right)$
X
0.1
0.2
0.3
0.4
100
10
1

Fig.12